were low binding affinities[12,31] and long metal ion to CO_2 carbon distances,[10,12,31] which would be more consistent with binding to a site other than the A site.

Further analysis of the MD trajectories has provided us with some qualitative insights that may have important implications for the function of the enzyme.[32] (1) The A site places the CO_2 molecule in such a way that it is "perfectly" aligned to react with the hydroxyl oxygen bound to the zinc ion at the active site (the CO_2 carbon to hydroxyl oxygen distance is 3.0 Å). Thus, given our observed structures, it appears likely that once CO_2 binds to this site it is nicely positioned to subsequently react to form the zinc-bicarbonate form of the enzyme.[32] (2) The Thr 199···HO-Zn hydrogen bond appears to be very strong and not fluxional. Thus, we have suggested that the function of this interaction is to "lock" the hydroxyl hydrogen in the zinc-hydroxide form of the enzyme in what we will call the down position. In this orientation the lone pairs on the hydroxyl bound to the zinc ion are pointing toward the CO_2 molecule bound in the A binding site. If this hydrogen-bonding interaction was not present one might imagine that the zinc bound hydroxyl would be able to freely rotate, thereby potentially interfering with CO_2 binding and subsequent reaction.[32]

Conclusions

With the aid of two 126-ps MD simulations we have identified two CO_2 binding sites in HCAII, which we have labeled as the A and E binding sites. Analysis of these trajectories demonstrates that the A site provides a rather restrictive environment for the CO_2 molecule while the E site is less so. Using free energy perturbation simulations we have evaluated the absolute free energy of binding for CO_2 interacting with these sites. We find that the A site has a greater free energy of binding (-3.37 kcal/mol) than the E site (-2.17 kcal/mol). While these binding free energies are not quantitatively correct when compared to experiment they make sense from a functional perspective. Thus, the A site one would expect to be the reactive pocket due to its proximity to the zinc ion, and therefore one might expect that it should have a greater binding affinity than does a more remote site like the E site.

Liang and Lipscomb[33] have recently studied this problem using MD simulations and they have identified a total of three binding sites in the HCAII active site, two of which are similar, but not identical with our A and E sites. The third site, which is further out in the active site cavity, we will label as the F site. The addition of other binding sites fits in with our proposal that more binding sites increase the ability of HCAII to bind and to diffuse CO_2 molecules into the A binding site.

Our results provide suggestions for site-directed mutagenesis experiments that could be performed in order to further our understanding of the catalytic mechanism of HCAII and, in particular, the step involving the association of CO_2 with the protein. For the E site one could mutate Ala 65 into a larger group that would fill up this pocket and inhibit CO_2 binding, while for the A site mutating Val 143 into a larger group would block off this site. We look forward to these experiments being done along with high-pressure X-ray studies aimed at addressing this issue.

Acknowledgment. We thank the Center for Academic Computing at the Pennsylvania State University for generous allocations of IBM 3090-600S computer time. Helpful discussions with U. C. Singh and B. Brooks are also acknowledged. We thank J.-Y. Liang and W. N. Lipscomb for providing a copy of their manuscript prior to publication. D. N. Silverman, S. Lindskog, and C. Fierke have provided numerous very helpful and insightful comments on this present work and their help and support is gratefully acknowledged. Helpful comments by one of the referees are also acknowledged. Coordinates for the A and E binding sites can be obtained via an anonymous ftp download. The internet address is 128.118.30.113 and the PDB format coordinates are in the pubs/HCAII directory.

(32) Merz, K. M., Jr. *J. Mol. Biol.* **1990**, *214*, 799.

(33) Liang, J.-Y.; Lipscomb, W. N. *Proc. Natl. Acad. Sci.* Submitted for publication.

Ab Initio Search for the Structure of the 4-Protoadamantyl Cation

R. Dutler, A. Rauk,* S. M. Whitworth, and T. S. Sorensen*

Contribution from the Department of Chemistry, University of Calgary, Calgary, Alberta T2N 1N4, Canada. *Received March 23, 1990*

Abstract: The 4-protoadamantyl cation region of the $C_{10}H_{15}^+$ potential energy hypersurface is searched by means of RHF-SCF calculations and the STO-3G, 6-31G, and (in part) 6-31G* basis sets. Two structures are found. The structure with C_s symmetry is postulated to be the primary intermediate in the solvolysis of 4-*endo*-protoadamantyl derivatives. It is calculated to be 8 kJ/mol less stable than the second structure which has no symmetry. The asymmetric cation is postulated to be the primary intermediate in the solvolysis of 4-*exo*-protoadamantyl derivatives. It is 7 kJ/mol less stable than 2-adamantyl cation to which rearrangement is hindered by a very small barrier. Rearrangement of the C_s structure is expected to be hindered by relatively large barriers. It may be generated directly from bicyclo[4.3.1]dec-3-en-8-yl derivatives. The C_s cation is characterized by IGLO calculations of ^{13}C and ^1H NMR chemical shifts.

Introduction

Solvolysis of 4-*exo*- and 4-*endo*-protoadamantyl derivatives proceeds[1] with an *exo*/*endo* reactivity ratio of $\sim 10^4$. The products of solvolysis of 4-*exo*-protoadamantyl 3,5-dinitrobenzoate were exclusively 2-adamantyl derivatives.[1] The rearrangement has been shown to proceed with retention of configuration of the oxygen moiety.[2] On the other hand, solvolysis of the 4-*endo* tosylate (*endo*-**1**-OTs) under some conditions gave predominantly 2-adamantyl derived products but also some 4-*endo*-protoadamantanol. No 4-*exo*-protoadamantanol was detected.[1] Acetolysis of 2-adamantyl tosylate (**2**-OTs) under buffered con-

(1) Lenoir, D.; Hall, R. E.; Schleyer, P. v. R. *J. Am. Chem. Soc.* **1974**, *96*, 2138-2147.

(2) Nordlander, J. E.; Haky, J. E. *J. Org. Chem.* **1980**, *45*, 4780.

0002-7863/91/1513-411$02.50/0

Scheme I

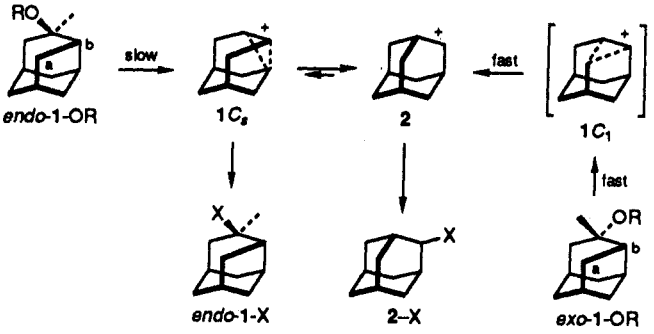

ditions yielded 0.4–0.5% of 4-*exo*-protoadamantyl acetate as well as the 2-adamantyl product,[1,3] but no 4-*endo* product.[3] Deamination of a 2-adamantyl derivative, **2**-NHN_2Ph, under acetolysis conditions also yielded 2-adamantyl acetate (**2**-OAc) as the major product, but also several percent of protoadamantene (**3**), 4-*exo*-protoadamantyl acetate (*exo*-**1**-OAc), and 2,4-dehydroadamantane (**4**). Isotopic labeling experiments associated with

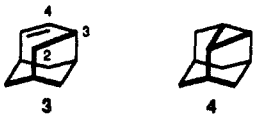

solvolysis experiments revealed H/D scrambling in the intermediate cation from 4-*endo*-protoadamantyl reactants but not from 4-*exo*-protoadamantyl derived starting materials.[4] The solvolysis, deamination, and isotopic labeling observations are consistent with Scheme I. Specifically, substantially different observations for the *exo*- and *endo*-4-protoadamantyl derivatives, the former being anchimerically assisted by bond a (Scheme I), the latter by bond b, suggest that more than one "4-protoadamantyl" cation may be involved.[1]

Entry into the 4-protoadamantyl cation system may also be gained by protonation of protoadamantene. The mechanism in aqueous media and in trifluoroacetic acid has been established to be rate-limiting protonation followed by rapid trapping of the intermediate cation (Ad_E2).[5] Addition of trifluoroacetic acid yields predominantly 2-adamantyl trifluoroacetate. A small amount of the 4-*exo*-protoadamantyl ester has also been detected.[6] It was determined that, under the solvolysis conditions, rearrangement of the 4-*exo* ester is too slow to account for the bulk of the major 2-adamantyl product, which must therefore have been produced directly.[6] Addition of deuterated trifluoroacetic acid to the alkene resulted in predominantly the exo disposition of the isotopic label, suggesting direct migration of the C_2–C_3 bond, or an intermediate with a nonclassical asymmetrically bridged structure, in the solvolysis.[6]

Figure 1 illustrates the relationship between the 2-adamantyl cation and possible 4-protoadamantyl cations. Classical structures best describe the bond migration which connects the "2-adamantyl" region of the $C_{10}H_{15}^+$ potential energy surface to the "4-protoadamantyl region". Experimentally, neither the 2-adamantyl cation nor the 4-protoadamantyl cation has been observed under stable ion conditions. In solvolysis reactions, products attributable to both species are obtained.

We describe herein an ab initio search for the structures of possible intermediates in the solvolysis of 4-protoadamantyl derivatives. Two possible intermediates are found.

Method

All geometry and energy determinations were carried out using either the GAUSSIAN 82[7] or the GAUSSIAN 86[8] systems of quantum chemistry

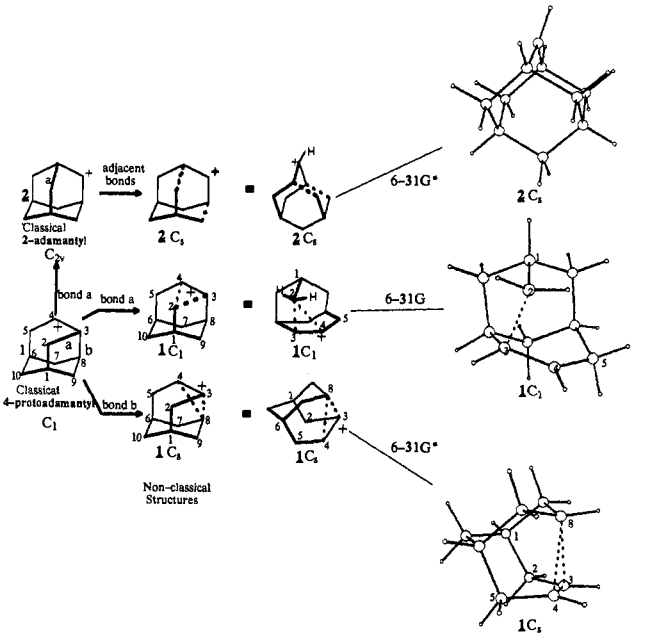

Figure 1. The relationship of the nonclassical 4-protoadamantyl cation structures to each other and to 2-adamantyl cation.

programs. Geometry optimizations were performed using the analytical gradient algorithms and internal basis sets. An exploration of the $C_{10}H_{15}^+$ potential energy surface in the vicinity of 4-protoadamantyl cation was initially carried out using the STO-3G basis set. Structures corresponding to stationary points were reoptimized at RHF/6-31G and, where possible, 6-31G* levels of theory. The nature of the stationary points, local minima or transition structures, was verified by analytical harmonic frequency analysis at the STO-3G- and 6-31G-optimized stationary points. It was not feasible to carry out frequency analysis with the 6-31G* basis set. Estimates for the effect of electron correlation error on the relative energies of the various structures are obtained to second order in Moller–Plesset perturbation theory using the 6-31G basis set (MP2/6-31G). The best estimate of relative energies were derived by adding the MP2/6-31G correlation energy correlation to the SCF 6-31G* energy at the 6-31G* geometry.

Calculations of the ^{13}C NMR chemical shifts were performed with the IGLO program[9] with the small internal Gaussian lobe basis (approximately equivalent to the 4-31G basis set of the GAUSSIAN programs).

Results and Discussion

The Level of Theory. The size of the 4-protoadamantyl system places severe limitations on the level of computational sophistication that can be brought to bear. Accordingly, a discussion of the consequences of use of less than ideal level of theory on the conclusions that can be drawn is in order. It is well-established in literature that is too vast to review that the description of carbocationic structures and bonding requires significantly higher levels of theory than is necessary for molecules which are not electron deficient. We will draw from computational experience with two systems relevant to the present study, 2-norbornyl cation[10–14] and 7-norbornenyl (and -dienyl) cation(s),[15] in order

(3) Storesund, H. J.; Whiting, M. C. *J. Chem. Soc., Perkin Trans. 2*, **1975**, 1452.
(4) Lenoir, D.; Schleyer, P. v. R. *J. Chem. Soc., Chem. Commun.* **1970**, 941–942.
(5) Allen, A. D.; Tidwell, T. T. *J. Am. Chem. Soc.* **1982**, *104*, 3145.
(6) Nordlander, J. E.; Haky, J. E. *J. Am. Chem. Soc.* **1980**, *102*, 7487.
(7) Binkley, J. S.; Frisch, M. J.; De Frees, D. J.; Raghavachari, K.; Whiteside, R. A.; Schlegel, H. B.; Fluder, E. M.; Pople, J. A. Department of Chemistry, Carnegie-Mellon University, Pittsburgh, PA.
(8) Frisch, M. J.; Binkley, J. S.; Schlegel, H. B.; Raghavachari, K.; Melius, C. F.; Martin, L. R.; Stewart, J. J. P.; Bobrowitz, F. W.; Rohlfing, C. M.; Kahn, L. R.; De Frees, D. J.; Seeger, R.; Whiteside, R. A.; Fox, D. J.; Fluder, E. M.; Pople, J. A. Carnegie-Mellon Chemistry Publishing Unit, Pittsburgh, PA, 1984.
(9) (a) Schindler, M.; Kutzelnigg, W. *J. Chem. Phys.* **1982**, *76*, 1819. (b) Schindler, M. *J. Am. Chem. Soc.* **1987**, *109*, 1020.
(10) Kohler, H.-J.; Lischka, H. *J. Am. Chem. Soc.* **1979**, *101*, 3479.
(11) Goddard, J. D.; Osamura, Y.; Schaeffer, H. F., III *J. Am. Chem. Soc.* **1982**, *104*, 3258.
(12) Raghavachari, K.; Haddon, R. C.; Schleyer, P. v. R.; Schaeffer, H. F., III *J. Am. Chem. Soc.* **1983**, *105*, 5915.
(13) Yoshimine, M.; McLean, A. D.; Liu, B.; DeFrees, D. J.; Binkley, J. S. *J. Am. Chem. Soc.* **1983**, *105*, 6185.
(14) Liu, B.; DeFrees, D. J. *J. Am. Chem. Soc.* **1989**, *111*, 1527.

Table I. Calculated and Relative Energies of 2-Adamantyl, 1-Adamantyl, and 4-Protoadamantyl Cations

	2-adamantyl				1-adamantyl		4-protoadamantyl		
	energy (hartree)			ΔE	energy	ΔE	energy (hartree)		ΔE
method	C_{2v}	$2C_s$	C_1	(kJ/mol)[a]	(hartree) C_{3v}	(kJ/mol)[a]	**1**-C_s	**1**-C_1	(kJ/mol)[a]
SCF/STO-3G//STO-3G	−382.678 280	−382.678 381		0.27			−382.644 879	−382.663 778	88.0 (38.4)
SCF/3-21G//STO-3G	−385.026 778	−385.027 420		1.69					
SCF/6-31G//STO-3G	−387.000 092	−387.000 611		1.36			−386.979 176	−386.992 019	56.3 (22.6)
SCF/6-31G//6-31G	−387.003 100	−387.004 167	−387.004 061	2.80 (0.26)	−387.020 589	−43.13	−386.988 620	−386.996 009	40.8 (21.5)
SCF/6-31G*//6-31G*	−387.162 516	−387.164 458		5.10	−387.180 304	−41.61	−387.148 415		42.1
MP2/6-31G//STO-3G							−387.874 547	−387.875 896	−3.5[c]
MP2/6-31G//6-31G	−387.879 744	−387.882 423	−387.882 407	7.04 (0.04)	−387.903 276	−54.77	−387.876 901	−387.879 886[d]	14.5 (6.7)
MP2/6-31G//6-31G*							−387.875 702		
MP2/6-31G*//6-31G*[b]		−388.042 714[b]					−388.037 107[b]		14.7

[a] Relative to 2-adamantyl **2**-C_s. [b] Estimated by adding the MP2/6-31G//6-31G* correlation energy correction to the SCF/6-31G*//6-31G* energy. [c] E(**1**-C_1) − E(**1**-C_s). [d] Correlation energy transfered from STO-3G geometry of **1**-C_1.

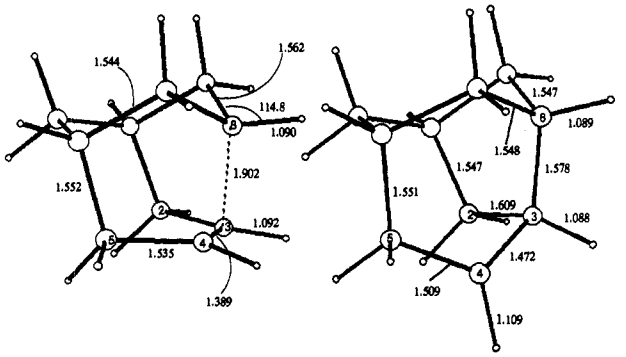

Figure 2. 4-Protoadamantyl cation: (left) STO-3G structure with enforced symmetry plane, **1**-C_s; (right) no symmetry constraint, **1**-C_1.

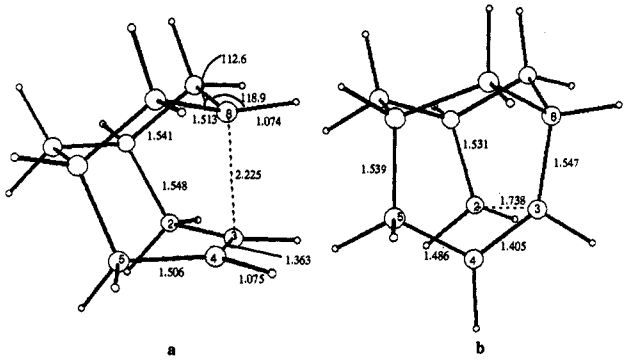

Figure 3. 4-Protoadamantyl structures at the 6-31G level: (a) **1**-C_s; (b) **1**-C_1.

to assess the "error limits" of the procedures used herein. SCF calculations using the minimal STO-3G basis set strongly favor "classical" structures,[10] "nonclassical" structures being preferentially stabilized using split-valence basis sets[11] (e.g., 3-21G or 4-31G) and especially by inclusion of electron correlation.[12,13] Calculations with nonpolarized split-valence basis sets yield geometries of symmetrical three-center, two-electron bonds which are too open or "π complex-like". Addition of polarization functions to the basis set (e.g., 6-31G*) reduces the bond distances significantly.[15] Further optimization with inclusion of correlation (MP2/6-31G*) yields little further change in the geometry[15] but a significant lowering of the energy relative to less bridged structures.[11-14] As 4-protoadamantyl cation **1** is too large for use with our present facilities even to evaluate the MP2 correlation correction at 6-31G*, we are forced to make a rough estimate at 6-31G and assume that *relative* correlation corrections at this level adequately approximate the results at higher level.

The total and relative energies of 4-protoadamantyl cation **1** as well as 2-adamantyl cation **2**[16] and 1-adamantyl cation[16] are listed in Table I. All energies are relative to the most stable form of **2**, unless indicated otherwise. Skeleton numbering in the figures is according to IUPAC for the classical structure of **1**. Results on **1** as obtained at different levels of theory are discussed separately below.

4-Protoadamantyl Cation. STO-3G Basis Set. 4-Protoadamantyl cation was optimized at the STO-3G level of theory with the constraint that the symmetry be C_s (**1**-C_s), and without any symmetry constraints (**1**-C_1). The geometries of the two structures are shown in Figure 2. At the SCF/STO-3G level, the **1**-C_s structure is 88.0 kJ/mol less stable than the 2-adamantyl cation **2** at the same level. Harmonic frequency analysis indicates that at this level of theory **1**-C_s is a *transition structure*. These results are as expected from similar calculations on the 2-norbornyl cation.[10-14] The normal mode with imaginary frequency is of A″ symmetry and involves a twisting motion of the "double bond" so as to move the structure toward a classical secondary cation of C_1 symmetry. It is of particular interest that significant deviations from the nonclassical bridging geometry of the cation which would dissociate the π complex do not occur until the 6th, 7th, and 9th normal modes (frequencies >500 cm^{-1}), at which point stretching motions of the long bonds, C_3–C_8 and C_4–C_8, are mixed with other skeleton deformation modes. The most notable feature of the STO-3G C_s structure is the long C_3–C_8 distance (1.902 Å) separating the formal secondary cation site from the π-bonded carbon atoms C_3 and C_4 which are separated by a "benzene-like" double-bonded distance (1.389 Å).

Optimization at SCF/STO-3G level without symmetry constraints yielded the **1**-C_1 structure shown in Figure 2 which is in effect a classical 4-protoadamantyl cation. **1**-C_1 is 40.5 kJ/mol less stable than the 2-adamantyl cation but 47.5 kJ/mol more stable than **1**-C_s. Harmonic frequency analysis confirms that at this level of theory **1**-C_1 is a local minimum. While the classical nature of the **1**-C_1 structure is not supported at higher levels of theory, numerical measurements of dihedral angles based on the skeleton shown in Figure 2b will prove useful for analysis of anchimeric assistance in the solvolysis of 4-protoadamantyl derivatives and possible rearrangement pathways, as discussed below.

4-Protoadamantyl Cation. 6-31G Basis Set. Optimizations were carried out with the 6-31G basis set in a manner parallel to the

(15) Bremer, M.; Schotz. K.; Schleyer, P. v. R.; Fleischer, U.; Schindler, M.; Kutzelnigg, W.; Koch, W.; Pulay, P. *Angew. Chem., Int. Ed. Engl.* **1989**, *28*, 1042.
(16) Dutler, R.; Rauk, A.; Sorensen, T. S.; Whitworth, S. M. *J. Am. Chem. Soc.* **1989**, *111*, 9024-9029.

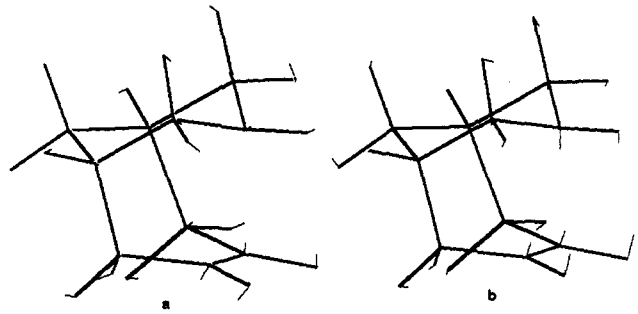

Figure 4. (a) Lowest frequency normal mode of 4-protoadamantyl cation **1**-C_s at SCF/6-31G//6-31G level, symmetry A″, frequency 159 cm^{-1}; (b) second lowest normal mode, symmetry A′, frequency 217 cm^{-1}.

STO-3G investigations. The C_s-constrained geometry is shown in Figure 3. The structure resembles, even more than the STO-3G structure, a π complex, since the C_3–C_8 distance is longer (2.225 Å) and the C_3–C_4 distance is shorter (1.363 Å). However, the split-valence basis set has had a dramatic effect on the energy relative to 2-adamantyl. Thus, **1**-C_s is 40.8 kJ/mol less stable than 2-adamantyl at this level, compared to 88.0 kJ/mol at the STO-3G level. The correlation correction (MP2/6-31G) for **1**-C_s is larger than for **2** and further narrows the separation. With the MP2/6-31G level correction energy included, **1**-C_s is only 14.5 kJ/mol less stable than **2**. It is expected that at higher levels of theory the difference between **1**-C_s and **2** would be even less.

Harmonic frequency analysis indicates that at the RHF/6-31G level of theory **1**-C_s is a *minimum*, not a transition structure as suggested by the STO-3G basis set results discussed above. The lowest normal mode is of A″ symmetry and involves a twisting motion of the "double bond" so as to move the structure toward a classical secondary cation. The normal mode is shown in Figure 4. It is of particular interest that, in contrast to the results with the STO-3G basis set, the next lowest normal mode involves the symmetric stretch of the nonclassical three-center two-electron bond. This normal mode is also shown in the Figure 4.

The 4-protoadamantyl cation was also optimized at the 6-31G level without any symmetry constraints, using the STO-3G **1**-C_1 (Figure 2) geometry and force constants as a starting point for the optimization. The resulting structure, shown in Figure 3, is qualitatively the same as the STO-3G **1**-C_1, except that the C_2–C_3 bond has stretched substantially and the C_3–C_8 bond has contracted to a normal length. The SCF energy is lower by 19.4 kJ/mol than the **1**-C_s structure. Thus, **1**-C_1 and **1**-C_s are confirmed as *separate* minima at the 6-31G level of theory. The MP2/6-31G correction for correlation error is not as important as for **1**-C_s. After inclusion of correlation energy estimate, **1**-C_1 is 7.8 kJ/mol below the **1**-C_s structure and only 6.7 kJ/mol above 2-adamantyl **2** at the same level. It is clear that the internal strain energy of either the **1**-C_s or the **1**-C_1 structure must be substantially less than the estimated difference in strain energy between protoadamantane and adamantane, 46 kJ/mol,[17] or between 4-protoadamantyl and 2-adamantyl acetate, 31 kJ/mol.[3]

Examination of the frontier molecular orbitals of **1**-C_1 (Figure 5) reveals the extent of the asymmetry in the electron-deficient bonding in the vicinity of the "cationic" region of the molecule. The HOMO-2 orbital shows an in-phase combination of the hybridized formally empty orbital on C_2 and a highly distorted C_3–C_4 π orbital. This interaction is more explicitly shown in the out-of-phase combination of these two local orbitals which makes up the LUMO (Figure 5). The distribution of the LUMO, which is concentrated mainly on C_4, suggests that addition of nucleophiles to **1**-C_1 should occur at C_4 from the *exo* side.

4-Protoadamantyl. 6-31G* Geometry. For practical reasons, 4-protoadamantyl cation could only be optimized at the 6-31G* level of theory with the constraint that the symmetry be C_s. The

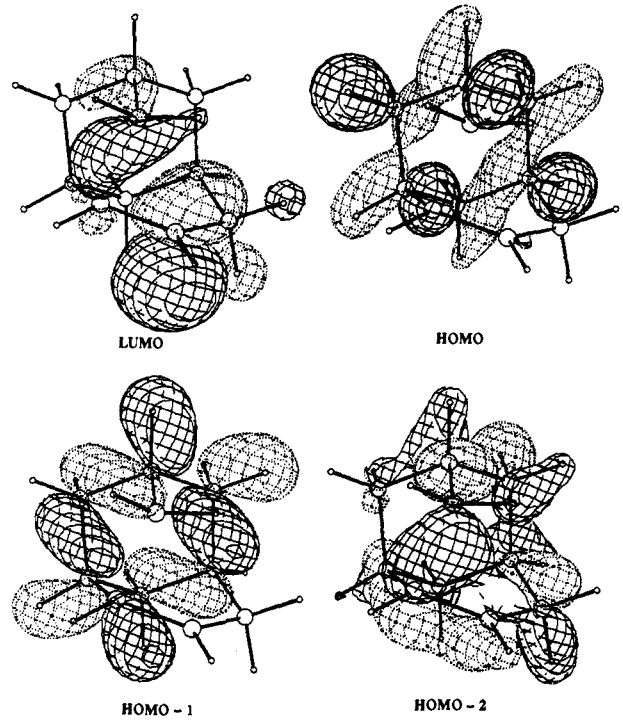

Figure 5. Higher occupied MOs and LUMO of asymmetric 4-protoadamantyl cation **1**-C_1: 6-31G geometry and basis set; contour value 0.05.

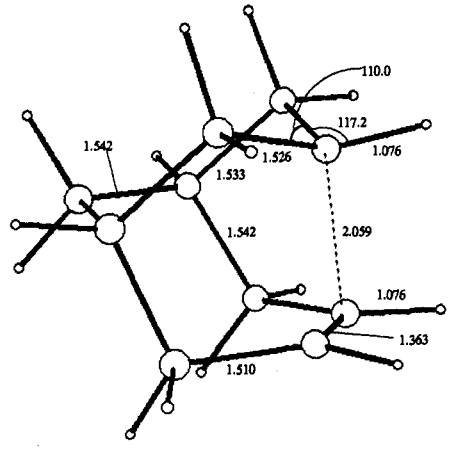

Figure 6. The 6-31g* geometry of 4-protoadamantyl cation **1**-C_s.

geometry is shown in Figure 6. With respect to the C_3–C_8 distance (2.059 Å), this structure falls between the STO-3G and 6-31G structures, as expected from the preliminary discussion. Experience with the 7-norbornenyl cation[15] suggests that reoptimization at MP2/6-31G* would not lead to significant changes in the geometry or calculated chemical shifts (see below). At the 6-31G* SCF level, **1**-C_s is 42.1 kJ/mol less stable than **2**. It was not feasible to obtain a MP2/6-31G* correlation energy. Consequently, the correlation error was estimated by MP2/6-31G calculation at the 6-31G* geometry for both **1**-C_s and **2**. As with the 6-31G geometry, the correlation correction is larger for 4-protoadamantyl cation than for 2-adamantyl cation. With the MP2/6-31G level correlation energy included, **1**-C_s is 14.5 kJ/mol less stable than **2**, a result almost identical with that found at the 6-31G geometries.

The HOMO and LUMO of the 6-31G* structure, expanded in the 6-31G basis set for comparison with Figure 5, are shown in Figure 7. These frontier orbitals are precisely what one would expect on the basis of a symmetrical π complex between a secondary cation (at C_8) and a double bond (C_3–C_4). Inspection of the LUMO should provide some indication of the site of reaction of **1**-C_s with nucleophiles. Since the LUMO appears about equally

(17) (a) Lenoir, D.; Raber, D. J.; Schleyer, P. v. R. *J. Am. Chem. Soc.* **1974**, *96*, 2149. (b) Engler, E.; Andose, J.; Schleyer, P. v. R. *J. Am. Chem. Soc.* **1973**, *95*, 8005.

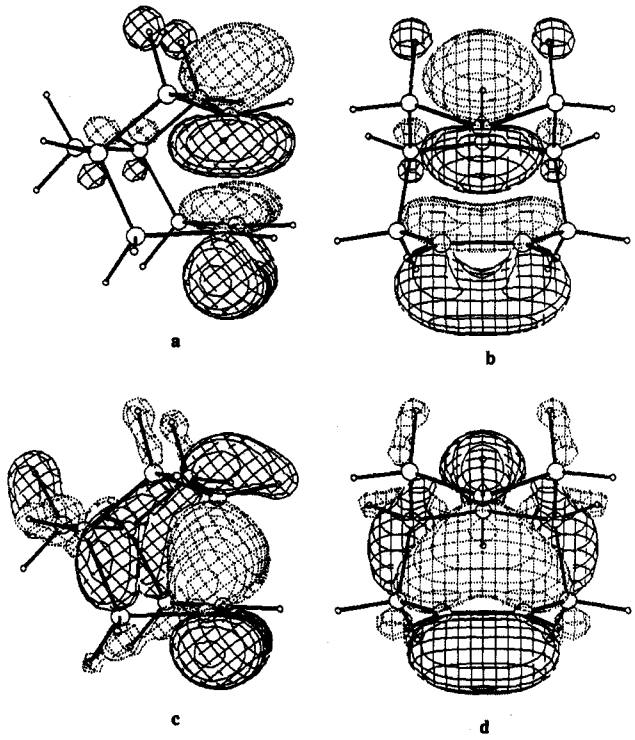

Figure 7. LUMO (a, b) and HOMO (c, d) of 4-protoadamantyl cation **1**-C_s at the 6-31G* geometry, basis set 6-31G, contour value 0.05.

distributed between the three centers, C_3, C_4, and C_8, one might expect to observe products from nucleophilic attack at all three centers. Addition to C_3 or C_4 would occur with equal probability and yield 4-*endo*-protoadamantyl derivatives, as observed.[1,4] Addition to C_8 would yield 8-*exo*-bicyclo[4.3.1]dec-3-ene (**5**)

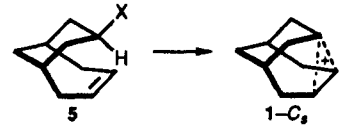

derivatives. Failure to observe **5** in solvolyses of **2**-X may be due to the instability of **5** under the reaction conditions.[18] Solvolyses of **5** have not been reported.

It was not possible because of resource limitations to optimize the structure at the 6-31G* level without symmetry constraints. However, one can infer from the similarities *in energy differences* between 6-31G and 6-31G* basis set results for the C_s structures that the results at the 6-31G* level for **1**-C_1 would not be much different from the 6-31G data shown in Table I. Thus, the computed results suggest the existence of two "4-protoadamantyl" structures, **1**-C_1 and **1**-C_s, with **1**-C_1 lower in energy than **1**-C_s, and both structures less stable that **2**, in accord with experimental evidence as discussed further below.

IGLO Chemical Shift Calculations on 1-C_s

The structure **1**-C_s is a potentially observable species for reasons discussed below. Recent work of Schleyer and co-workers[15,19-22] has established that IGLO calculations of ^{13}C NMR chemical shifts serve as a sensitive probe of structure of carbocations. IGLO calculations with the DZ basis set were carried out on **1**-C_s

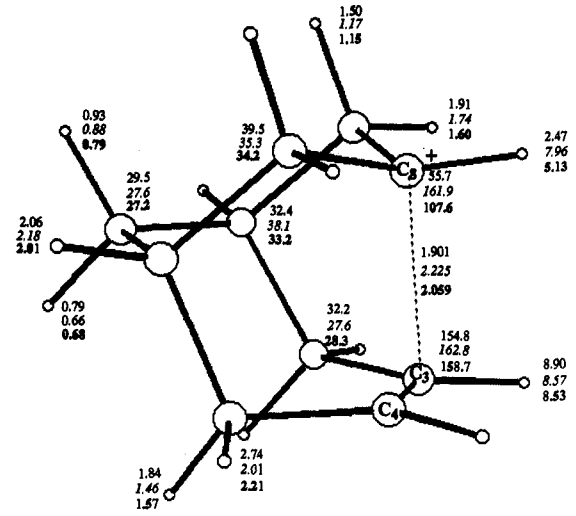

Figure 8. IGLO ^{13}C and ^{1}H chemical shifts of 4-protoadamantyl cation **1**-C_s: STO-3G; *6-31G*; **6-31G***. The numbers on the C_3–C_8 bond are in angstroms; all other numbers are chemical shifts, in ppm relative to TMS, of the associated atoms.

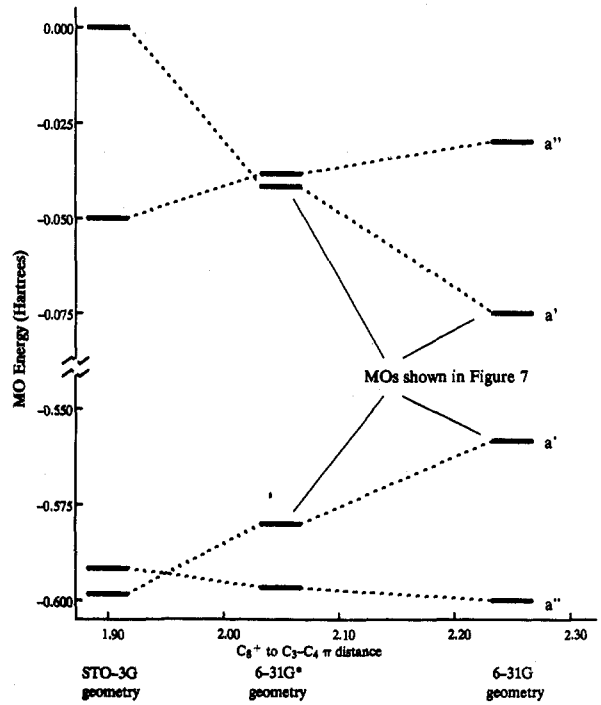

Figure 9. Frontier orbital correlation diagram for **1**-C_s: MO energies (6-31G) as a function of C_8^+ to C_3–C_4 π distance (see Figure 8).

structures of 4-protoadamantyl cation obtained by STO-3G, 6-31G, and 6-31G* optimization. These structures differ principally in the distance separating the secondary cationic centre from the "π" bond, C_3–C_8 separations being 1.901 Å, 2.225 Å, and 2.059 Å, respectively. The true structure of the species should fall in this range. The ^{13}C and ^{1}H chemical shifts in ppm relative to TMS are shown in Figure 8. The most striking features of the NMR chemical shifts calculated for the three structures are the great sensitivity and near-linear dependence of the chemical shifts on the separation of the formal secondary cation center from the C_3–C_4 π bond. A rationale may be found by examining the higher occupied and lower unoccupied MOs of the three structures, calculated with a common basis set (6-31G). The frontier orbitals of the 6-31G* structure are shown in Figure 7. The HOMO and LUMO are the in- and out-of-phase combinations, respectively, of 2p and π orbitals expected of a π complex. The LUMO + 1 and HOMO − 1 frontier orbitals (not shown) are combinations of C–C and C–H antibonding and bonding orbitals, respectively,

(18) Anchimeric assistance in the solvolysis of the related 7-norbornenyl chloride causes a rate increase of about 10^{11} over 7-norbornyl chloride.[23]

(19) Schleyer, P. v. R.; Laidig, K. E.; Wiberg, K. B.; Saunders, M.; Schindler, M. *J. Am. Chem. Soc.* **1988**, *110*, 300.
(20) Saunders, M.; Laidig, K. E.; Wiberg, K. B.; Schleyer, P. v. R. *J. Am. Chem. Soc.* **1988**, *110*, 7652.
(21) Schleyer, P. v. R.; Carneiro, J. W. de M.; Koch, W.; Raghavachari, K. *J. Am. Chem. Soc.* **1989**, *111*, 5475.
(22) Carneiro, J. W. de M.; Schleyer, P. v. R.; Koch, W.; Raghavachari, K. *J. Am. Chem. Soc.* **1990**, *112*, 4064.
(23) Winstein, S.; Ordronneau, C. *J. Am. Chem. Soc.* **1960**, *82*, 2084.

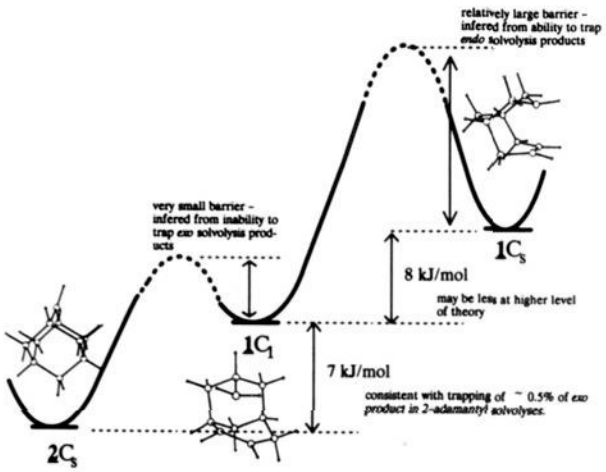

Figure 10. Summary of the experimental and computational observations of the 4-protoadamantyl and 2-adamantyl cation systems. The energy differences are best estimates based on the ab initio calculations. See the text for a discussion.

and are associated with the backbone of the ion rather than the cationic site. A plot of the frontier MO energies (6-31G) against the C–C separation, shown in Figure 9, reveals that the two highest occupied MOs and the two lowest unoccupied MOs cross over at a separation of about 2 Å.

Conclusions

Experimental observations and calculations suggest the energy profile shown in Figure 10 connecting the 4-protoadamantyl and 2-adamantyl regions of the $C_{10}H_{15}^+$ potential energy hypersurface. Two "4-protoadamantyl" cation minima were found. The existence of two separate minima is consistent with solvolysis and isotopic labeling results. Capture of the **1**-C_s structure would lead to *endo* products as found experimentally. Capture by the **1**-C_1 structure would lead to *exo* products. Small amounts of *exo* products have been observed from 2-adamantyl solvolyses. Solvolyses of 4-*endo*-protoadamantyl derivatives deuterated in the 4 position results in 1:1 scrambling of the label between C_3 and C_4, as expected from a symmetrical intermediate cation (**1**-C_s). Similarly labeled 4-*exo* derivatives exhibit no scrambling, all of the deuterium being found in the 1 position of the resulting 2-adamantyl derivative, consistent with the rapid rearrangement of an unsymmetrical cation (**1**-C_1). The ability to trap *endo* solvolysis products suggests that the **1**-C_s structure is separated from **1**-C_1 by a relatively large barrier. Conversely, the failure to observe deuterium scrambling or to trap *exo* solvolysis products suggests that **1**-C_1 is separated from **2** by a relatively low barrier.

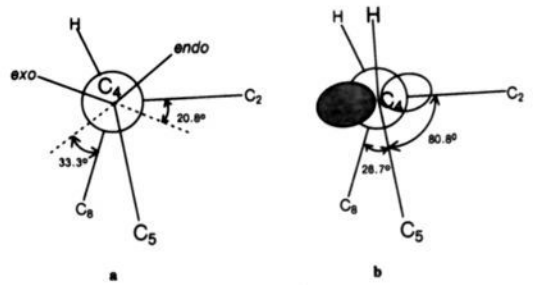

Figure 11. Relationship of the skeletal framework to: (a) the bonds at the 4 position of protoadamantane and (b) the nearly planar cationic site in classical **1**-C_1 (STO-3G geometry).

Inspection of the local geometry, shown in Figure 11a, of the protoadamantane skeleton in the region of C_4, as inferred from the STO-3G structure of **1**-C_1 suggests a possible reason that solvolysis of the 4-*endo* derivatives is much slower than for the 4-*exo* derivatives. Anchimeric assistance for the *endo* isomer by the C_8–C_3 bond is less efficient than for the *exo* by the C_2–C_3 bond owing to a less favorable alignment of the bonds. The dihedral angle between the C_8–C_3 bond and the departing *endo* substituent is about 33°, whereas the C_2–C_3 bond is only 21° out of alignment with the bond to a departing *exo* substituent. These conclusions are substantially the same as previously discussed by Schleyer and co-workers[1] on the basis of structures derived from molecular mechanics calculations.

The "classical" nature of the STO-3G **1**-C_1 structure (Figure 11b) may also be regarded as suggestive of the relative magnitudes of the **1**-C_1 → **2** and **1**-C_1 → **1**-C_s barriers. The rearrangement **1**-C_1 → **2** requires migration of the C_2–C_3 bond to C_4, a process which would be greatly facilitated by the nearly ideal orientation of the bond orbital to the vacant 2p orbital at C_4. On the other hand, the rearrangement **1**-C_1 → **1**-C_s requires migration of the C_8–C_3 bond to C_4, a process rendered difficult by the unfavorable orientation of the C_8–C_3 bond to the cationic site (Figure 11b).

An alternate route to **1**-C_s, namely, via the 8-X-bicyclo-[4.3.1]dec-3-ene system, appears not to have been investigated. The fact that **1**-C_s may be separated from **1**-C_1 (and **2**) by a relatively larger barrier offers some hope for its possible observation under stable ion conditions. The results of the IGLO calculations, which proved to be very sensitive to structural details, should assist in identification of the species.

Acknowledgment. Financial support for this work was provided by the National Sciences and Engineering Research Council of Canada. The provision of generous amounts of CPU time on the CDC Cyber 205 by SuperComputer Services is gratefully acknowledged.